JEE Journal of Ecological Engineering

Journal of Ecological Engineering, 25(12), 244–260
https://doi.org/10.12911/22998993/194494
ISSN 2299–8993, License CC-BY 4.0

Received: 2024.09.17
Accepted: 2024.10.20
Published: 2024.11.01

Fluoride Adsorption by Coffee-Ground Biochar Functionalized with Hydrogen Peroxide

Hellem Victória Ribeiro dos Santos[1], Renata Medici Frayne Cuba[1], Paulo Sérgio Scalize[1], Francisco Javier Cuba Teran[1*]

[1] School of Civil and Environmental Engineering, Federal University of Goiás, Goiânia GO, Brazil

* Corresponding author's e-mail: paco@ufg.br

ABSTRACT

Groundwater contains high levels of dissolved ions, which pose health risks when consumed. This study proposes biochar production for fluoride (F^-) removal from aqueous solutions using sustainable materials and functionalization processes.Biochar derived from coffee grounds carbonization at 500 °C was functionalized with hydrogen peroxide (H_2O_2). Structural morphology analysis utilized SEM+EDS, BET, and BJH techniques, while XRD and FTIR analyses assessed surface chemistry. Effects of pH, dosage, and initial F^- concentration on adsorption were evaluated, along with kinetics and thermodynamics.H_2O_2 increased acid functional groups on the surface without significantly altering surface area or pore volume. The highest adsorption capacity (0.179 mg g^{-1}) and removal efficiency (25.5%) were at pH = 4. Kinetic studies highlighted the influence of initial F^- concentration on adsorption equilibrium time and capacity. Experimental data fitting to pseudo-second-order and Elovich models suggested chemical mechanisms predominance, with intraparticle diffusion as the rate-limiting step. Adsorption isotherm fitting to Langmuir and Freundlich models indicated physical and chemical processes combination. The highest adsorption capacity was recorded at 1.46 mg g^{-1} at 55 °C. Thermodynamic analysis revealed endothermic and non-spontaneous nature, potentially affecting F^- affinity towards the adsorbent.

Keywords: defluoridation, fluoride; adsorbent, water treatment, fluorosis, dental caries.

INTRODUCTION

Approximately one-third of the world's population relies on underground water sources for their supply [1]. Despite being perceived as a safe source by most users [2], it can naturally contain elevated concentrations of dissolved ions such as sodium (Na^+), magnesium (Mg^{2+}), nitrate (NO_3^-), and fluoride (F^-) due to direct contact with geological formations [3]. Fluoride, along with nitrate and arsenic, are inorganic chemical compounds that typically occur in high concentrations in groundwater, with their excessive consumption posing significant health risks, hence limited to 1.5 mg L^{-1} [4].

Occurrences of F^- in groundwater above recommended concentrations have been documented worldwide [3, 5–7]. Various methods have been proposed to adjust F^- concentrations to recommended levels, including precipitation using ultra-pure compounds as seeds for accelerating the crystallization process [8], reverse osmosis [9], electrocoagulation using aluminum electrodes [10], and electrodialysis [11]. However, these methods may have limitations, including high operational and maintenance costs, potential for secondary pollution from toxic byproducts, and complex operational procedures [12]. In contrast, the adsorption technique employing powdered activated carbon (PAC) [13] is highly favored due to its satisfactory results, lower cost, and simplicity of design and operation compared to other treatment methods [14].

Nevertheless, using PAC as an adsorbent presents environmental challenges, mainly because it is typically sourced from nonrenewable coal [15] and involves high production costs [16], which can make it commercially impractical.

Consequently, alternative adsorbent materials to PAC, such as biochar, have gained increased attention since 2005 [17].

Biochar, characterized by its porous and carbon-dense nature, is generated through the carbonization of cellulosic or noncellulosic biomass in environments with restricted or no oxygen [18]. In addition to its lower production cost compared to PAC, biochar offers high precursor material availability and is environmentally sustainable [19]. Various raw materials, including agricultural residues, woody agro-industrial residues, and biosolids, can be utilized for biochar production, with lignocellulosic residues being the most prevalent in the literature likely due to their higher lignin content, which correlates with increased production yield and fixed carbon content in biochar [20]. However, biochar possesses limited properties such as small pore size and low surface functionality, which may restrict its efficacy in water treatment as these properties influence contaminant adsorption [21]. Consequently, there is an escalating need to obtain materials with enhanced sorption characteristics to substitute PAC in advanced water treatment [22]. The surface chemistry and morphological characteristics of biochar significantly influence its properties, with precursor feedstock and biochar surface activation being crucial determinants [20].

Coffee residues, which are rich in organic compounds such as oxygen, hydroxyl, carboxyl, amino, sulfonic, and phenolic functional groups [23], can effectively adsorb inorganic compounds like fluoride. They are a promising raw material for biochar production due to their substantial global output (6×10^6 tons per year) [24]. However, research on using biochar derived from coffee grounds for anion removal is limited [25]. When such studies are available, the biochar typically undergoes functionalization with acid, basic, or oxidizing compounds, which alters its chemical or surface structure. This process increases the number of oxygen-containing functional groups that can form specific bonds with the adsorbate, such as hydrogen bonding and π-π electron donor–acceptor interactions [26], or incorporating compounds with opposite charges to the anion into biochar, resulting in electrostatic interactions [25].

The utilization of biochar derived from coffee residues has garnered attention in various studies focused on anionic pollutant removal such as phosphate and nitrate [24, 25] and radioactive iodine [27].

While studies on F^- adsorption using coffee ground biochar are scarce, there have been reports on the production of functionalized biochar from coffee grounds [28, 29]. Surface chemistry functionalization was suggested to enhance F^- adsorption, advocating for environmentally less aggressive products [28]. Hydrogen peroxide (H_2O_2) has emerged as a promising agent for biochar functionalization due to its cost-effectiveness and environmentally benign nature [30]. Studies have shown that treatment with H_2O_2 increases the presence of acid, carboxyl, and hydroxyl functional groups on the biochar surface, which can improve F^- adsorption due to the affinity of F^- for acid biochars [31–33].

The aim of the current study is the production of biochar from coffee grounds and functionalization with hydrogen peroxide (H_2O_2) at 30 vol for F-removal. The physicochemical characterization of biochar surfaces was conducted, and batch tests were performed to evaluate the impact of operational parameter.

MATERIALS AND METHODS

Materials and reagents

Ultrapure water (1.35 $\mu S\cdot cm^{-1}$) produced in an LA 023 GEHAKA Master All Ultrapurifier was used in all experiments. Analytical grade reagents were utilized. Sodium fluoride (NaF) reagent solutions were prepared for the adsorption assays. Fluoride (F^-) analysis was conducted using an 18AF ion-selective fluoride electrode, Analyzer® 550 M, with samples previously filtered through quantitative filter paper.

Coffee grounds were collected by brewing coffee without adding any substances like sugar or sweeteners. Ultrapure water was used to wash the coffee grounds at 80 ± 5 °C, and after that they were rinsed at room temperature (26 °C ± 5 °C) [35]. Finally, they were dried in an oven (105 °C ± 5 °C) for 24 h and kept in a desiccator until use.

Biochar preparation and surface functionalization

Biochar without functionalization (BC pristine) was produced in a rotary bipartite tubular furnace (Sanchis®) heated to 500 °C (10 °C min^{-1}) for 2 h under a nitrogen flow (200 $mL\cdot min^{-1}$) [28]. To prepare functionalized biochar (FBC), 1 g of pristine

biochar (BCP) was agitated in a rotating chamber (110 rpm) at room temperature with 20 mL of H_2O_2 (30 vol) for 2 h [36]. The FBC was washed with ultrapure water, then dried in an oven at 105 °C for 24 h. BCP served as a control for FBC in characterization and adsorption studies.

Physical-chemical characterization

The adsorbent materials were characterized using various methods, including the determination of the pH at the point of zero charge (pH_{ZCP}) by the 11-point method [37]. Additional characterization techniques included morphological surface analysis, elemental analysis, X-ray diffraction (XRD), fourier transform infrared spectroscopy (FTIR), specific surface area analysis (BET), total pore volume, and mean diameter distribution (BJH). These parameters were determined using nitrogen (N_2) adsorption-desorption isotherms at -195.85 °C.

Adsorption tests

Analyses of pH, adsorbent dosage, temperature, adsorption capacity, and rate of F^- adsorption were performed. Adsorption kinetics were evaluated, considering the influence of the initial F^- concentration. All experiments were conducted in batches using a refrigerated shaker incubator set at a consistent speed of 100 rpm, with the temperature maintained at 22 °C ± 1 °C. When necessary, pH adjustments were made using 0.1 M HCl or NaOH solutions.

The influence of pH was assessed by adding 0.5 g of adsorbent to 50 mL of NaF solution (7 $mg \cdot F^- \cdot L^{-1}$) with pH values ranging from 2 to 12. Adsorbent dosages from 0.1 g to 2.0 g were added to 50 mL of NaF solution (7 $mg \cdot F^- \cdot L^{-1}$, pH 2). The suspensions were agitated for 24 hours, and outcomes were quantified in terms of fluoride removal efficiency and adsorption capacity. Equilibrium time and the influence of initial F^- concentration were evaluated. Solutions with initial concentrations of 7.0, 15.0, and 30.0 $mg \cdot F^- \cdot L^{-1}$ at pH 2 were agitated with 10 $g \cdot L^{-1}$ of adsorbent. Aliquots were collected at predetermined intervals for analysis. Kinetic parameters were obtained by fitting data to pseudo-first order, pseudo-second order, Elovich, and Webber-Morris models [38, 39]. The adsorption capacity was assessed using 10.0 $g \cdot L^{-1}$ of adsorbent at the previously mentioned temperature in 50 mL of NaF solution, with concentrations of 1.5, 3.0, 7.0, 14.0, and 30.0 $mg \cdot F^- \cdot L^{-1}$ at pH 2. Following a 5-hour incubation period, the concentration of F^- was measured, and adsorption capacity values were determined utilizing the Langmuir and Freundlich adsorption isotherm models [40].

Thermodynamic parameters (ΔG°, ΔH°, ΔS°) were calculated using Gibbs, van't Hoff, and the plot of lnKd vs. 1/T equations based on adsorption isotherm tests conducted at 35 °C, 45 °C, and 55 °C [41].

RESULTS AND DISCUSSION

Physicochemical characterization of BCP and FBC

The pH of FBC was 5.08, lower than the pH of BCP (6.74). This pH decrease after functionalization aligns with findings by [42], who reported a decrease in pH from 8.30 to 5.82 after oxidation with H_2O_2 (10% w/v). The decrease in pH observed after functionalization can be linked to the generation and/or enhancement of carboxylic groups on the surface of the FBC, which possess mildly acidic properties [36, 43].

Figure 1 displays the XRD spectrum of FBC. The sharp 2θ diffraction peak near 25° indicates the presence of a phase abundant in carbon with minimal crystallinity [44]. The peak observed around 44° is indicative of the (100) plane in the graphitic crystal lattice of carbon, suggesting minimal or absent stacking order among the small graphene planes [45]. Compared to [46], who produced biochar from coffee grounds at 300 °C, no peak associated with cellulose crystallographic planes near 20° was observed. The absence of this peak study suggests a high degree of cellulose degradation in FBC, likely due to the carbonization temperature used (500 °C) leading to total biomass stabilization [35]. The same behavior was observed for BCP.

As illustrated in Figure 2A to Figure 2D, the surface structure comparison between BCP and FBC shows that both surfaces exhibit a rough and heterogeneous texture, containing pores of various shapes and sizes.

It is also notable that FBC exhibits a greater abundance of free pores compared to BCP, likely due to the corrosive action of the oxidizing agent, facilitated by an acid mixture (CH_3COOH + H_3PO_4, 1:1), used to modify the biochar [47].

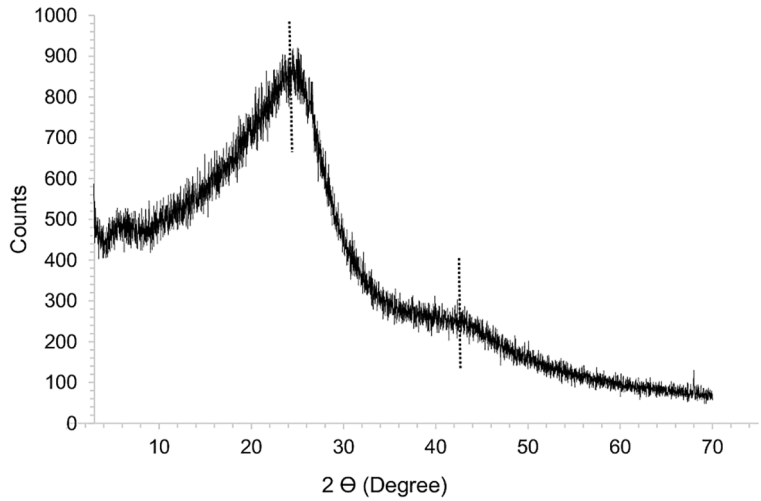

Figure 1. X-ray diffractogram

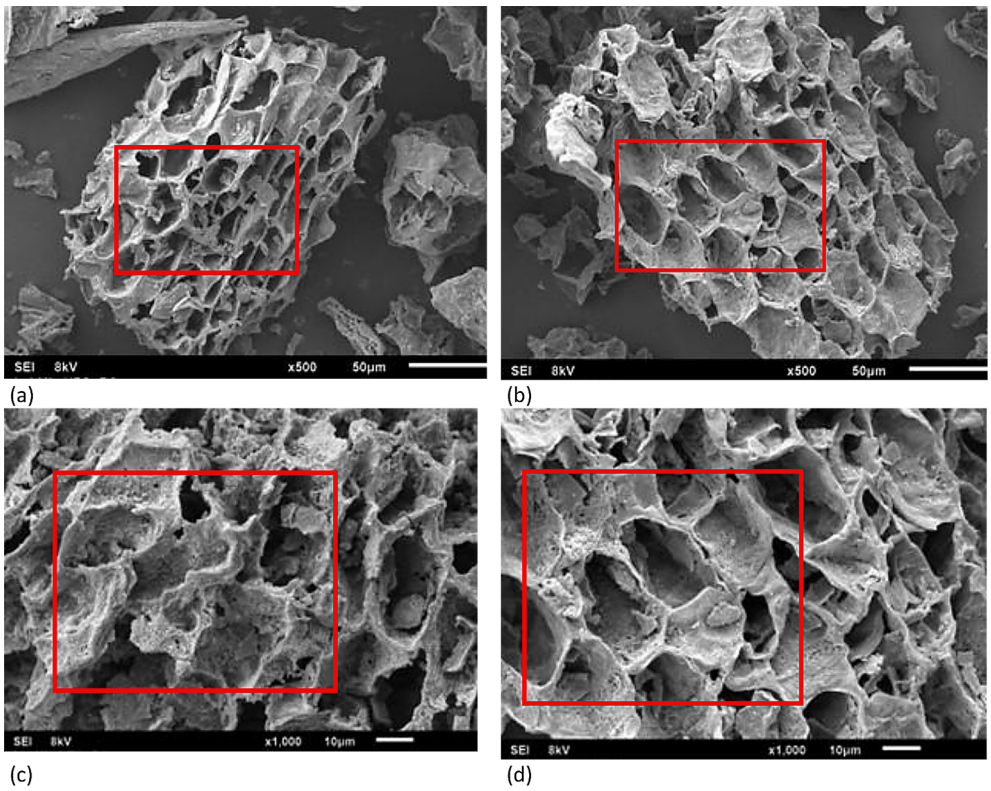

Figure 2. Photomicrographs of BCP samples (a) and (c) and BCFs (b) and (d). Images (a) and (c) depict the surface of BCP with emphasis on clogged pores, while images (b) and (d) highlight free pores after treatment with H_2O_2

The presence of particles blocking pores suggests relatively inferior pore properties in BCP [48].

The EDS spectrum in Figure 3 indicates a predominant presence of carbon in BCF, along with smaller quantities of oxygen, magnesium, aluminum, potassium, and calcium. Similarly, EDS analysis of biochar produced from spent coffee grounds, pyrolyzed at 500 °C for 2 hours, also showed the presence of Mg and Ca [49]. These elements have the potential to form complexes with fluoride ions or precipitate [50]. Comparable results were obtained for BCP.

As depicted in Figure 4, the analysis of N_2 adsorption and desorption isotherms at -195.85 °C for FBC revealed that these isotherms fall under type III classification. In such isotherms, the adsorbed

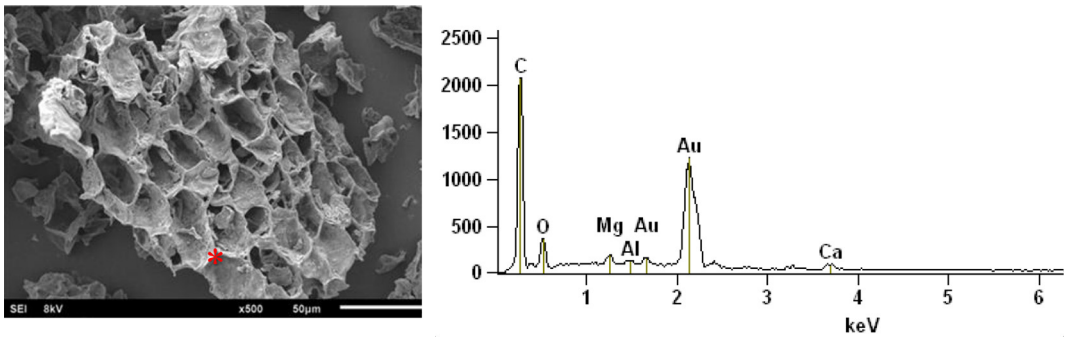

Figure 3. Energy dispersive spectroscopy of the FBC. *Incidence point of the electron beam; magnification of 350X

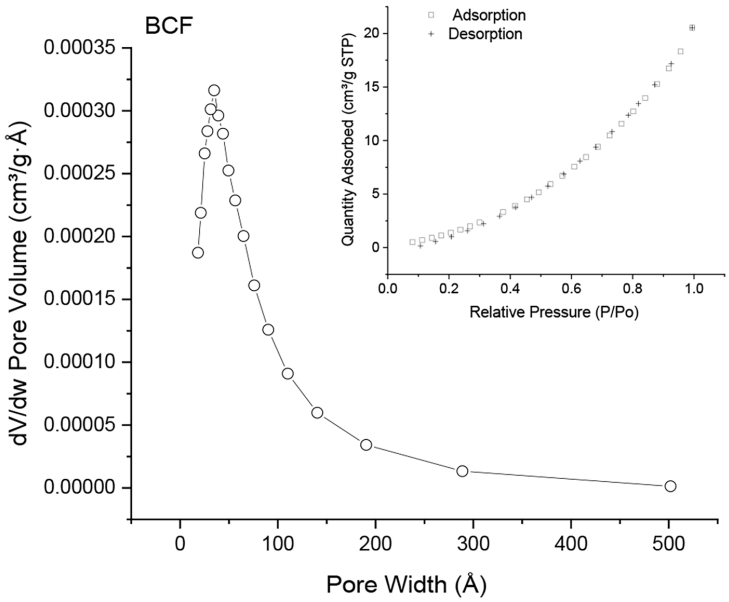

Figure 4. N_2 adsorption and desorption isotherms (-195.85 °C) for FBC

molecules aggregate around the most favorable sites on the solid surface, which include pores of varying sizes [51].

The largest observed pore volume in the samples had a diameter of approximately 35 Å mesopore equivalent [51], exceeding the radius of F, which measures 1.33 Å [38], and its ion hydrated state at 3.52 Å [19]. The BET surface area of FBC was 12.7 $m^2 \cdot g^{-1}$, with a corresponding pore volume of 0.0318 $cm^3 \cdot g^{-1}$. For BCP, these values were 12.94 $m^2 \cdot g^{-1}$ and 0.0349 $cm^3 \cdot g^{-1}$, respectively. These findings indicate that under the applied conditions, H_2O_2 did not generate or notably modify the pore structure of BCP to augment its surface area [52]. Nonetheless, others [53] suggested that porosity had minimal impact on F^- removal, with acid surface groups primarily responsible for F^- removal. Figure 5A compares BCP spectra with FBC spectra before adsorption, while Fig. 5B compares FBC spectra before and after adsorption. Regarding functional groups, the FTIR spectrum following functionalization with hydrogen peroxide, depicted in Figure 5A, revealed a significant enhancement in the intensity of bands associated with oxygenated functional groups such as -OH and -CO (3418 cm^{-1}, 1589 cm^{-1}, and 1383 cm^{-1}), which are highly effective in binding F^- ions [54]. On the other hand, in Figure 5B a comparison between pre and post absorption on functionalized BC.

In both spectra, at 3418 cm^{-1}, a representative band of O–H stretching exhibited decreased intensity after F^- adsorption, indicating interactions via hydrogen bonds during the adsorption process [55], consisted with finding in similar studies [56]. At 1383 cm^{-1}, a band attributed to C–OH deformation associated with the oxygenated group was detected, which became more intense

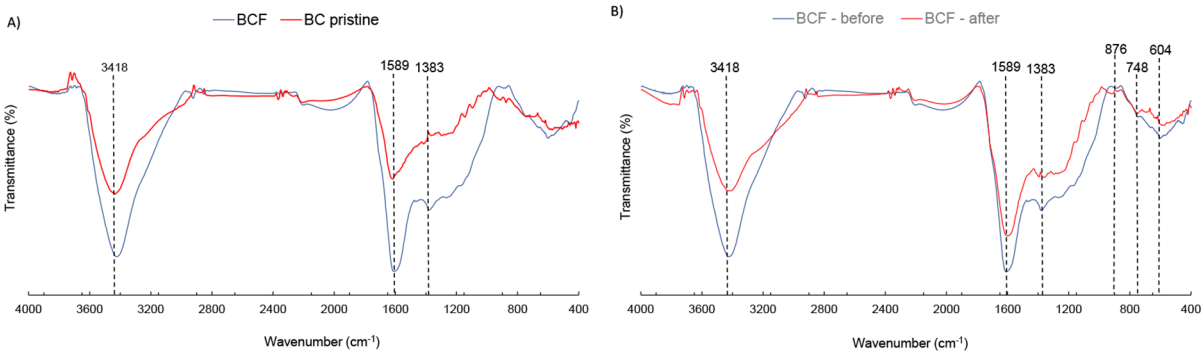

Figure 5. Infrared spectra of BCP and FBC a) and FBC before and after adsorption of F^- (b)

after functionalization, indicating the insertion of oxygen groups. However, after F^- adsorption, this band weakened due to electrostatic interactions between F^- and protonated OH groups (OH_2^+), which are primarily responsible for F^- adsorption [57]. The prominent peak at 1589 cm^{-1} (within the range of 1565 cm^{-1} to 1600 cm^{-1}) indicated the overlap of the stretching vibration mode (–C=C) of the aromatic ring of carbon with absorption bands attributed to carboxylic groups, esters, lactones, and carbonyls (–C=O) [58]. The bands observed at 876 cm^{-1} and 748 cm^{-1} are indicative of calcium and magnesium compounds, respectively [59], along with the band at 604 cm^{-1}, which is characteristic of calcium oxides [60]. Overall, the spectra depicted in Figure 5 suggest that following adsorption, there was a decrease in the intensity of the bands and/or a shift in their positions, confirming the adsorption of F^- on the FBC [61].

Effect of initial pH and adsorbent dosage

Figure 6A and Figure 6B illustrate the adsorption capacity at equilibrium (qe) and the removal efficiency of F^- from the BCP and FBC samples, respectively, in response to variations in initial pH. pH influenced significantly both the adsorption capacity and F^- removal efficiency. For BCP, the highest value of efficiency was 20.6% and the highest value of adsorption capacity was 0.124 $mg \cdot g^{-1}$ at pH = 2.0, while for FBC, they were 0.179 $mg \cdot g \cdot g^{-1}$ and 25.5%, respectively at pH = 4.

The enhanced adsorption capacity at acidic pH values reinforces the mechanism of F^- adsorption through interactions with protonated OH groups (OH_2^+), as indicated by the analysis of the FTIR spectra. Equations 1 and 2 elucidate the process [54].

$$-COH + H^+ \leftrightarrow COH_2^+ \quad (1)$$

$$-COH_2^+ + F^- \leftrightarrow CF + H_2O \quad (2)$$

However, elevated pH levels are linked to a reduction in both removal capacity and efficiency, likely due to competition between fluoride ions and hydroxyl ions for the available adsorption sites [44, 62, 63]. Another consideration is that at basic pH values, the surface of both adsorbents becomes negatively charged due to the pH_{ZCP} values of BCP (4.76) and FBC (3.85), promoting electrostatic repulsion of F-ions [45], which are predominant in the medium due to the low pK value of HF (3.17). Because BCP served as a

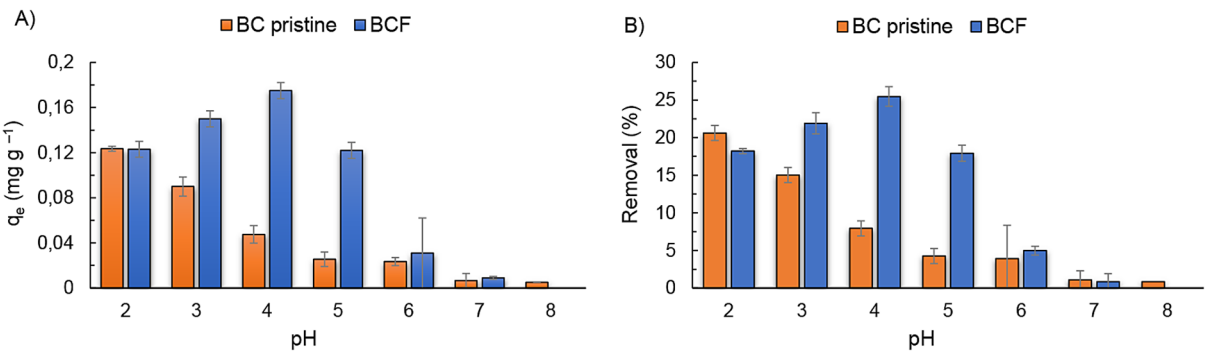

Figure 6. Equilibrium adsorption capacity a) and F^- removal, b) for BCP and FBC as a function of pH

control for FBC and due to the minor difference in adsorption capacity between BCP and FBC at pH 2.0, adsorption characterization tests were conducted at this pH for both adsorbents.

Adsorption capacity and F^- removal are shown in Figure. 7A and Figure 7B for BC and FBC, respectively, plotted against adsorbent mass.

The adsorption capacity of biochar depends on the presence of active functional groups and pores on its surface [64]. Consequently, the removal efficiency increased with higher doses (Fig. 7A). However, a similar trend was not observed for the adsorption capacity (qe) because as the mass increased, F^- ions selectively adsorbed onto lower energy sites, leading to surface nonsaturation [38].

The adsorption capacity of biochar relies on the presence of active functional groups and pores on its surface [64]. Consequently, the removal efficiency of both adsorbents increased with higher doses (Fig. 7A). However, a similar trend was not observed for the adsorption capacity (qe) because as the mass increased, F^- ions selectively adsorbed onto lower energy sites, leading to surface nonsaturation [38].

BCP exhibited superior F^- removal performance regardless of the dosage. The highest adsorption capacity for BCP was 0.358 $mg \cdot g^{-1}$ at a 2 $g \cdot L^{-1}$ adsorbent dose, whereas for FBC, it was 0.0308 $mg \cdot g^{-1}$ at a 40 $g \cdot L^{-1}$ adsorbent dose. Additionally, the F^- adsorption capacity showed minimal variation with increasing FBC mass; for doses of 0.5 g, 1.0 g, and 2.0 g, the qe values obtained were equal to 0.026 $mg \cdot g^{-1}$, 0.028 $mg \cdot g^{-1}$, and 0.031 $mg \cdot g^{-1}$, respectively. Based on these results, adsorption tests were conducted using a dosage of 0.5 g of adsorbent, equivalent to 10 $g \cdot L^{-1}$.

F^- adsorption kinetics

For both adsorbents, irrespective of the initial fluoride concentration (as shown in Fig. 8), the adsorption kinetics displayed two distinct phases:

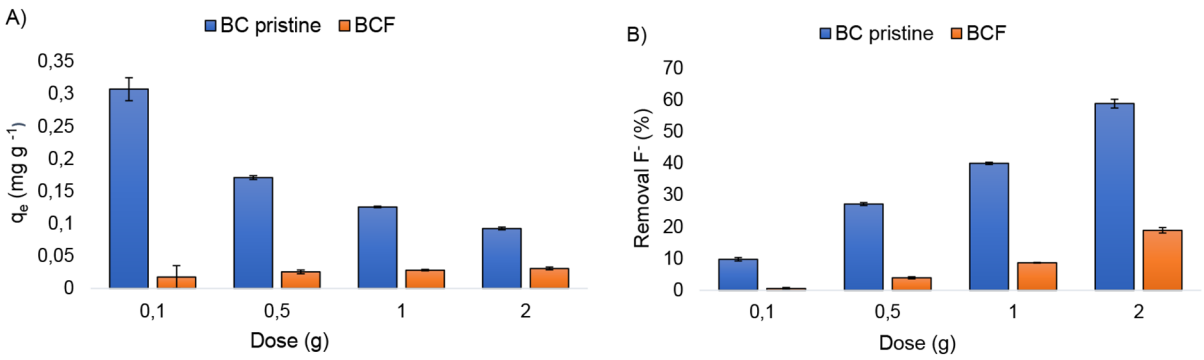

Figure 7. a) Adsorption capacity b) fluoride removal

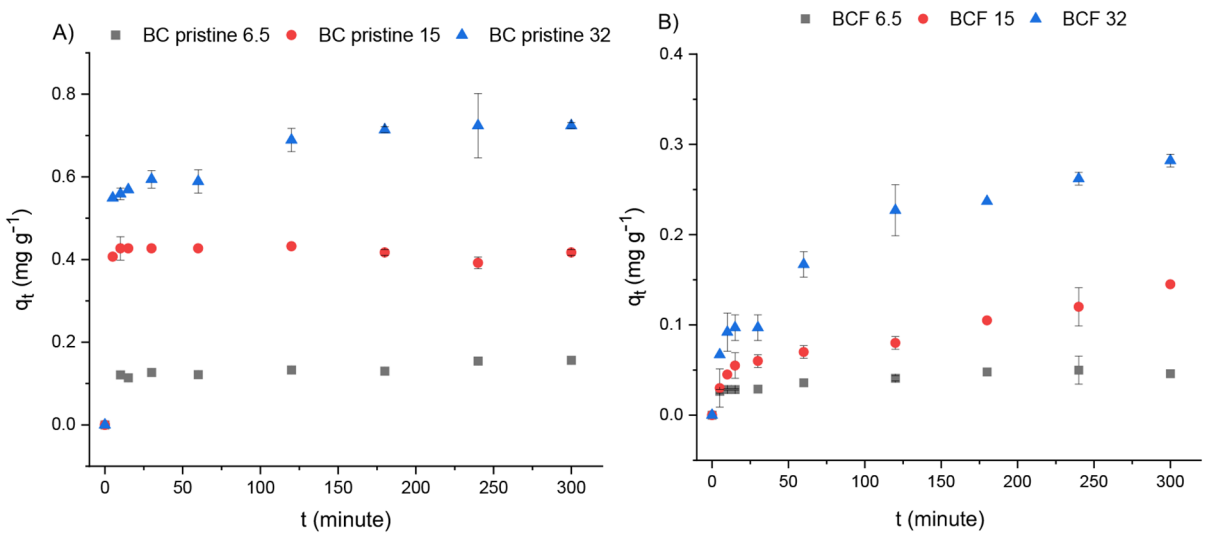

Figure 8. For initial concentrations F^- ranging equal to 6.5 mgL^{-1}, 15 mgL^{-1} and 32 mgL^{-1}, graphs show the adsorption capacity of pristine biochar BC a) and FBC b) over the time

a rapid initial phase followed by a slower phase until equilibrium was attained. This pattern is consistent with previous studies on fluoride removal using biochar derived from maize [40]. The initial rapid adsorption rate can be attributed to the concentration gradient between the solute in solution and the adsorbent, driven by the abundance of available adsorption sites [38].

Removal capacities of 0.121 $mg \cdot g^{-1}$ for concentration of 6.5 $mg \cdot L^{-1}$, 0.407 $mg \cdot g^{-1}$ for concentration of 12.0 $mg \cdot L^{-1}$, and 0.569 $mg \cdot g^{-1}$ for concentration of 32,0 $mg \cdot L^{-1}$, occurred in the initial 15 min for BC as shown in Fig. 8A. Equilibrium was attained within 30 min for concentrations of 6.5 $mg \cdot L^{-1}$ and 12.0 $mg \cdot L^{-1}$, while for a concentration of 32.0 $mg \cdot L^{-1}$, it took 180 min to reach equilibrium. In contrast, for FBC (Fig. 8B), assays with the same concentrations achieved the highest removal rates within the first 15 min, with values of 0.03 $mg \cdot g^{-1}$ and 0.06 $mg \cdot g^{-1}$, respectively, reaching equilibrium after 180 min. For the initial F^- concentration of 32.0 $mg \cdot L^{-1}$, the removal rate was 0.23 $mg \cdot g^{-1}$ at 120 min, with equilibrium reached after 300 min. Notably, for FBC, the increase in the concentration of F^- only significantly influenced the adsorption rate after 30 min of testing. This observation may be associated with the predominant adsorption mechanism. In this context, the adsorption kinetics are pivotal for illustrating the process of mass transfer from the solute to the solid–liquid interface, facilitating a better understanding of the removal mechanism involved [41].

As shown in Figure 9, due to the higher adsorption capacity observed, the pseudo-first-order (PFO), pseudo-second-order (PSO), and Elovich models were employed to analyze the data from tests using solutions with a concentration of 32.0 $mg \cdot L^{-1} \cdot F^-$.

The experimental data for both adsorbents fitted better to the PSO and Elovich models, as indicated by the R^2 values and the close similarity between the equilibrium adsorption capacity predicted by the models and the experimentally obtained values presented in Table 1.

The PFO model adequately fits the experimental data only during the initial 30–50 mins. Conversely, the PSO model thoroughly characterizes the entire adsorption process by accounting for external liquid film diffusion, surface adsorption, and intraparticle diffusion [65]. Its fitting to the data signifies the predominance of chemical mechanisms in the adsorption process [41]. As described by PSO models, the reaction rate is influenced by the quantity of solvent adsorbed on the adsorbent surface and the equilibrium adsorption amount. Under these conditions, the adsorption rate is directly proportional to the square of

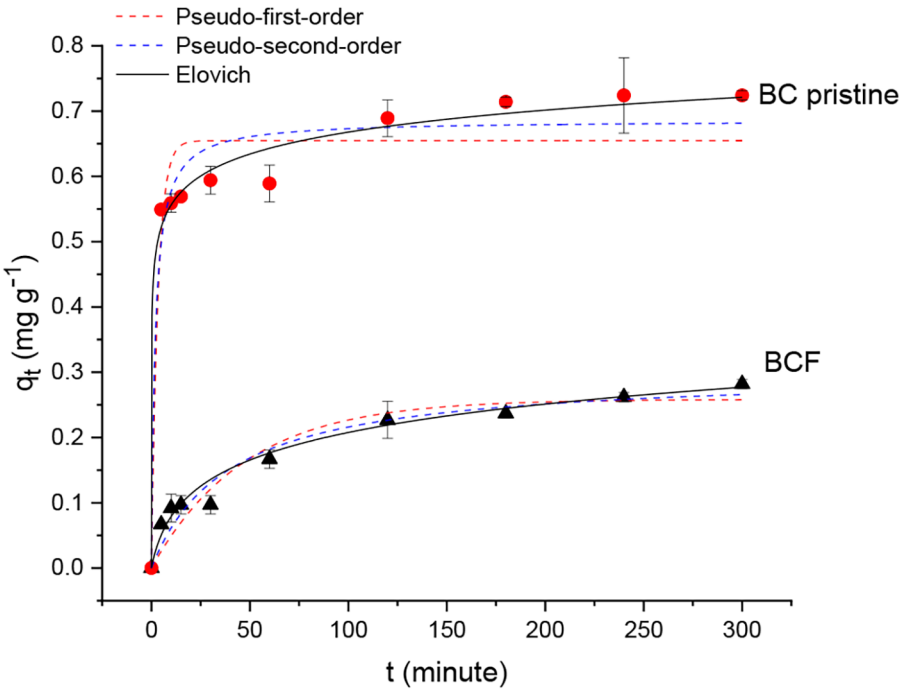

Figure 9. Fit of the results obtained in the adsorption kinetics test for the PFO, PSO and Elovich models. 6 hours of agitation at 100 rpm, 22 °C, pH = 2 (duplicate).

Table 1. Kinetic parameters for BC and FBC

Parameter	Unit	BCP	FBC
$q_{e\ (exp)}$	$mg \cdot g^{-1}$	0.721	0.260
Pseudo-first order			
$q_{e\ (calc)}$	$mg \cdot g^{-1}$	0.654	0.258
k_1	min^{-1}	0.3	0.021
R^2		0.91668	0.91572
Pseudo-second order			
$q_{e\ (calc)}$	$mg \cdot g^{-1}$	0.686	0.25
k_2	$mg \cdot g^{-1}\ min^{-1}$	0.771	0.08526
R^2		0.95579	0.95205
Elovich			
α	$mg \cdot g^{-1}$	457.4258	0.01543
β	$g \cdot mg^{-1}$	20.465985	15.4728
R^2		0.98881	0.98491

the number of unoccupied active sites on the surface, while the number of occupied active sites correlates with the adsorbate concentration [66].

Numerous studies have recognized that PSO kinetics is the most appropriate model for characterizing fluoride (F^-) removal in the adsorption process [45, 67, 68]. Additionally, the high R^2 value obtained for the Elovich model, along with confirming the predominance of the PSO model, suggests the energetically heterogeneous nature of the surfaces of the studied solids [45]. The obtained α and β values for BCP (457.426 $mg \cdot g^{-1}$ and 20.466 $g \cdot mg^{-1}$) and FBC (0.015 $mg \cdot g^{-1}$ and 15.47 $g \cdot mg^{-1}$), respectively, indicate that in BCP, adsorption occurs faster than desorption ($\alpha >> \beta$), whereas in FBC, the desorption rate surpasses adsorption, indicating a lower affinity of F for the adsorbent surface ($\alpha << \beta$) [69]. These results align with the lower qe values obtained for FBC.

To gain further insights into the adsorption mechanism, the intraparticle diffusion model, also known as the Weber–Morris model, was employed. This model explains the transport of the adsorbate from the solution to the adsorbent surface, with pore diffusion being the limiting step of the adsorption process [67, 70]. For this analysis, qt data over time were plotted against the square root of time (Fig. 10).

For BCP, F^- adsorption occurs in two stages. The initial stage is primarily due to the rapid diffusion of F^- from the bulk solution to the external surface or boundary layer of BCP. The subsequent stage is characterized by intraparticle diffusion, where F^- ions are adsorbed at active sites on the inner surface of the adsorbent [71].

In this subsequent stage, the reduced slope of the linear segment signifies greater hindrance in F^- diffusion within the pores, owing to the diminished concentration of these ions in the solution, which results in inadequate mass transfer [72]. Since the segments do not intersect at the origin, it suggests that the adsorption of F^- ions follows a complex process characterized by multiple steps, where intraparticle diffusion is not the limiting factor. [73].

Three stages were discerned for FBC. The initial and second stages unfolded similarly to BCP, involving immediate diffusion of F^- from the bulk solution to the external surface of FBC and subsequent diffusion of F^- ions from the adsorbent surface into

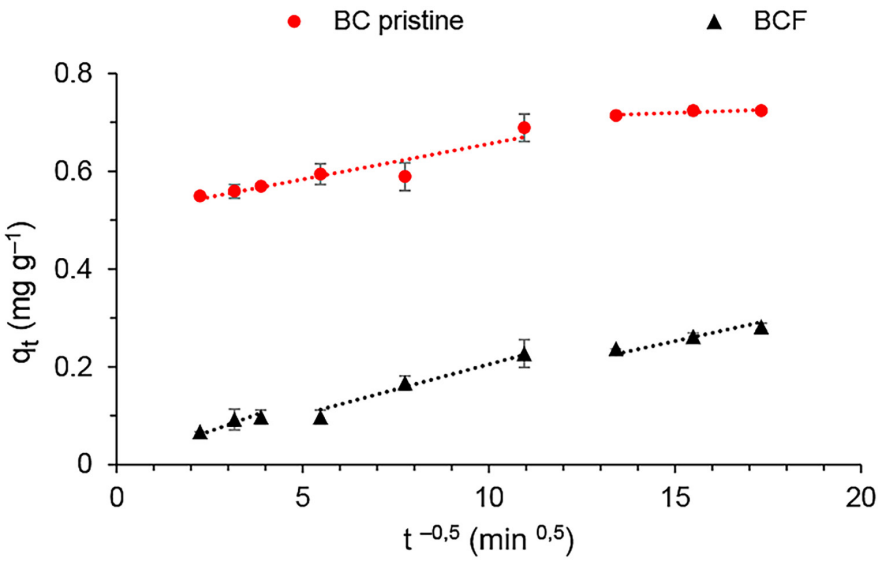

Figure 10. Data fitting for the intraparticle diffusion model

the inner pores along the pore walls (intraparticle diffusion). In the third stage, F^- ions are adsorbed onto the interior surface of the adsorbent [74]. Given that all three linear segments passed through the origin, it indicates that intraparticle diffusion constitutes the limiting step of the process [75].

The intraparticle diffusion model fit resulted in R^2 values of 0.966 for FBC and 0.53 for BCP. The kd and C parameters for FBC and BCP were 0.016 ($mg \cdot g^{-1} \cdot min^{-0.5}$) and 0.028, and 0.026 ($mg\ g^{-1} \cdot min^{-0.5}$) and 0.365, respectively. A higher kd value for BCP indicates a faster F^- diffusion rate compared to FBC, whereas lower C values suggest a lesser impact on the limiting boundary layer [73]. These data explain the lower adsorption rates obtained for FBC than for BCP.

The influence of temperature on F^- adsorption was investigated for BCP (Fig. 11A) and FBC (Fig. 11B) at concentrations of 1.5, 3.0, 7.0, 14.0, and 30.0 $mg \cdot F^- \cdot L^{-1}$. It was observed that for initial F^- concentrations of 1.5 $mg \cdot L^{-1}$ and 3.0 $mg \cdot L^{-1}$, increasing the temperature did not influence the F^- adsorption capacity for either adsorbent. However, at a concentration of 7.0 $mg \cdot L^{-1}$, a rise in temperature led to an increase in adsorption capacity, particularly for BCP, and this effect was even more pronounced at an initial F^- concentration of 30.0 $mg \cdot L^{-1}$. For BCP (Fig. 11A), the qe value rose from 0.262 $mg \cdot g^{-1}$ to 0.555 $mg \cdot g^{-1}$ when the temperature increased from 35 °C to 55 °C. In comparison, for FBC, qe increased from 0.03 $mg \cdot g^{-1}$ to 0.104 $mg \cdot g^{-1}$ over the same temperature range. The variation in qe values, from 35 °C to 55 °C, represents a 2.1-fold increase in adsorption capacity for BCP and a 3.5-fold increase for FBC. This indicates that the F^- adsorption process for both adsorbents is endothermic and that FBC is more responsive to temperature changes than BCP. Similar F^- adsorption behavior was reported for aluminum trichloride-modified biochar derived from corn stalks [40], where the authors noted that solution temperature impacts physicochemical surface adsorption, intraparticle diffusion rate, and internal chemical interactions.

To better understand the adsorption equilibrium, the F^- adsorption capacity results were modeled using adsorption isotherms. These models help elucidate the distribution of the adsorbate between liquid and solid phases and determine the adsorbent's capacity [75]. Figure 12 presents the fit of the experimental data to the Langmuir and Freundlich models.

The Langmuir model characterizes monolayer chemical adsorption, where the adsorbate binds to finite adsorption sites with constant energy and without the mobility of adsorbent molecules on the surface [75]. Conversely, the Freundlich model posits that adsorption occurs on an energetically heterogeneous surface, indicating that the heat of adsorption varies among the molecules adsorbed on the adsorbent surface [76].

Table 2 presents the parameters related to the Langmuir and Freundlich models for both BCP and FBC at temperatures of 55 °C, 45 °C, and 35 °C.

Except for the test performed with FBC at 35 °C, all adjustments for both adsorbents at the three temperatures studied showed $R^2 > 0.91$. This result suggested that the adsorption of F^- on the adsorbents occurs through a combination of multiple processes, including physical and chemical adsorption [40].

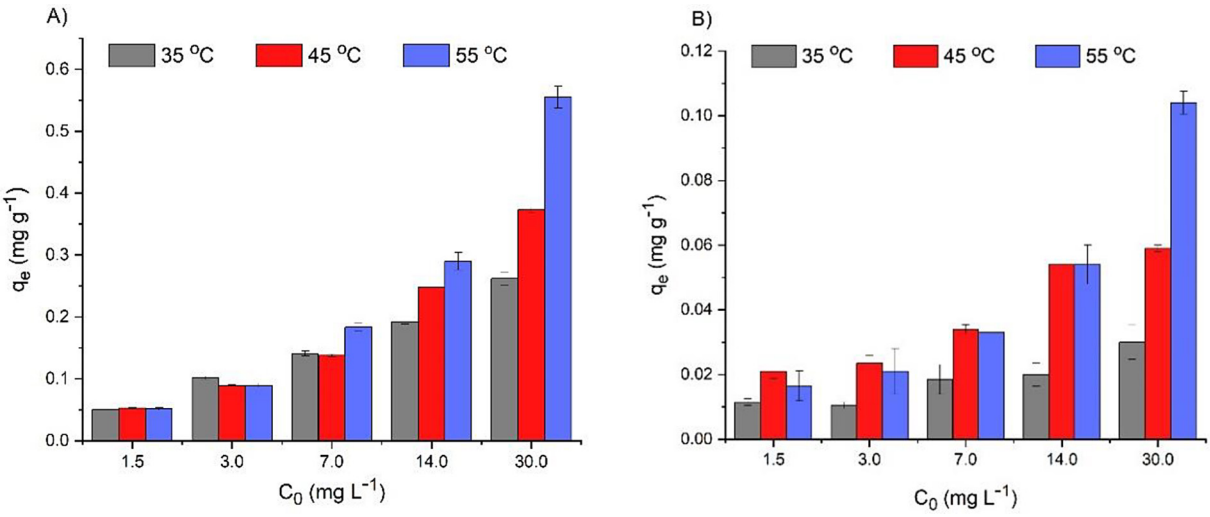

Figure 11. F^- adsorption capacity of BCP a) and FBC b) at different temperatures

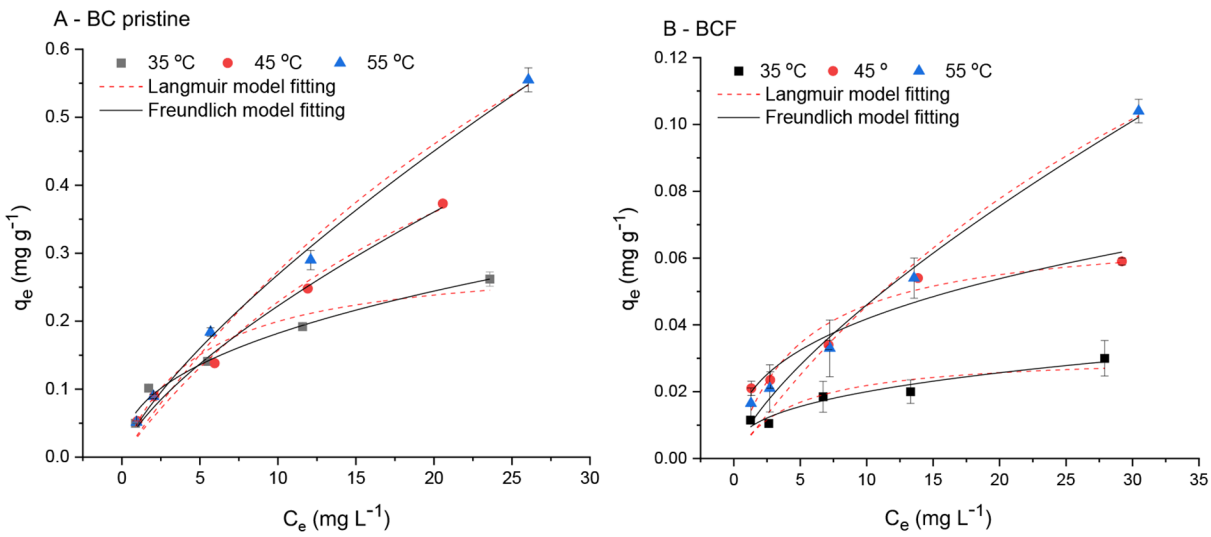

Figure 12. Adsorption isotherms of F^- on BCP a) and FBC b) at different temperatures

Table 2. Freundlich and Langmuir parameters of fluoride adsorption at different temperatures

Isothermal model	Temperature (°C)	Parameter	BCP	FBC
Freundlich	35	K_F	0.02966	0.00371
		n	0.42365	0.36064
		R^2	0.98311	0.94029
	45	K_F	0.04362	0.0129
		n	0.69749	0.36534
		R^2	0.99093	0.94052
	55	K_F	0.04817	0.0263
		n	0.7402	0.71673
		R^2	0.99645	0.98654
Langmuir	35	q_{max}	0.29601	0.03114
		K_L	0.20684	0.23508
		R^2	0.94469	0.82393
	45	q_{max}	0.85235	0.06863
		K_L	0.3659	0.20194
		R^2	0.97433	0.91904
	55	q_{max}	1.45727	0.26296
		K_L	0.02309	0.02101
		R^2	0.98715	0.96843

To assess the adsorption affinity of fluoride ions F^- by the adsorbents, the Langmuir constant (K_L) and the initial concentration of fluoride (Co) were utilized to calculate the separation factor (R_L), as given by Equation 3.

$$R_L = 1/(1 + K_L \cdot C_0) \quad (3)$$

For BCP, the RL values at temperatures of 55 °C, 45 °C, and 35 °C ranged from 0.590 to 0.966, 0.08 to 0.645, and 0.139 to 0.763, respectively. For FBC, the RL values were between 0.124 to 0.739, 0.141 to 0.767, and 0.613 to 0.969, respectively. According to the literature, RL values within the range of 0 < RL < 1 indicate favorable adsorption, with lower RL values reflecting a stronger interaction between the adsorbent and the adsorbate [54]. Additionally, as RL decreased with increasing initial F^- concentration, it was observed that anion adsorption on the studied biochars improved with higher F^- concentrations [76]. This relationship, along with the dependence of adsorption on the initial F^- concentration,

was further supported by the Freundlich constant (n) values being less than 1, indicating the favorable nature of the adsorption process [77].

Table 3 compares the q_{max} values obtained in this study with those reported in the literature. As shown in Table 2, according to the Langmuir model, the lower qmax values for FBC, compared to BCP, corroborate the results obtained from the Elovich kinetic model, indicating a higher affinity of F^- for BCP than for FBC.

In a previous study [32], biochar produced from sunflower husk was chemically modified with H_2O_2. The authors found that this modification did not significantly alter the adsorption capacity for tetracycline, with values of 7.26 $mg \cdot g^{-1}$ for pristine biochar and 7.93 $mg \cdot g^{-1}$ for modified biochar. The major change observed was surface oxidation of the biochar, which, despite increasing the content of oxygen-containing groups, also obstructed the pores, similar to the findings of the current study.

Generally, the q_{max} values reported in the literature are higher than those obtained in this study. However, it is important to note that fluoride adsorption is highly dependent on its initial concentration, which was higher in many of the referenced studies, thus explaining the lower values observed here. Furthermore, when activating agents include metals, particularly aluminum and iron, the difference is more pronounced. The presence of metals reduces the electrostatic repulsion between the biochar surface and F^- ions, thereby enhancing the adsorption capacity in aqueous solutions [61].

Adsorption thermodynamics

A thermodynamic analysis was conducted to evaluate the effect of temperature on the adsorption of F^- ions in both BCP and FBC. The study assessed temperatures of 35 °C (308 K), 45 °C (318 K), and 55 °C (328 K). Given that the Freundlich isotherm model best described the experimental data, the Kd from this model was used to calculate the thermodynamic parameters [83]. The thermodynamic parameters Gibbs free energy (ΔG°), enthalpy (ΔH°), and entropy (ΔS°) are presented in Table 4.

Table 3. Maximum adsorption capacity according to the Langmuir model from various studies

Adsorbent/Treatment	q_{max} ($mg \cdot g^{-1}$)	T (°C)	C_0 de F^- ($mg \cdot L^{-1}$)	Reference
BC coffee grounds/pristine	0.296 0.852 1.457	35 45 55	1.5 – 30.0	This study
BC coffee grounds/H_2O_2	0.031 0.069 0.263	35 45 55	1.5 – 30.0	This study
Activated carbon (GAC)	0.55	25	2.5 -10.0	[66]
BC pinecones/$FeCl_3$ BC pinecone/$AlCl_3$	9.95 12.10	25 25	0.5 – 40.0	[78]
BC corn stalk/$AlCl_3$	73.51 74.14 81.65	15 25 35	10.0 – 100.0	[40]
BC of wood residue (*T. hispida*)/$LaCl_3$	164	50	20.0 – 70.0	[79]
BC wood residues/$FeCl_3$	7.81 9.04 7.58	25 35 45	1.0 – 60.0	[80]
BC Kenaf (*Hibiscus cannabinus*)/$AlCl_3$	13.93	25	5.0 – 150.0	[38]
BC Raw sawdust/formaldehyde BC sugarcane bagasse/H_2SO_4 BC produced from raw wheat straw/ formaldehyde	1.73 1.15 1.93	28	2.5- 15.0	[81]
BC Pine tree sawdust/H_3PO_4	0.885	25	10.0 – 300.0	[82]

Table 4. Fluoride adsorption thermodynamic parameters of F^- for BCP and FBC

T (K)	K_d		ΔG ($kJ\ mol^{-1}$)		ΔS ($kJ\ mol^{-1}K^{-1}$)		ΔH ($kJ\ mol^{-1}$)	
	BC	FBC	BC	FBC	BC	FBC	BC	FBC
308	0.02966	0.00371	9.0085	14.3316	0.1121	0.0363	20.4849	20.2812
318	0.04362	0.0129	8.2811	11.50215				
328	0.04817	0.0263	8.2710	9.9213				

The positive ΔH values, 20.4849 kJ·mol^{-1} for BCP and 20.2812 kJ·mol^{-1} for FBC, along with the increase in Kd values with rising temperatures, indicate that the F^- adsorption process is endothermic between 35 °C and 55 °C. Higher temperatures boost the kinetic energy of the adsorbate molecules, enhancing heat and mass transfer [83]. This aligns with the higher adsorption capacities observed at increased temperatures. Additionally, ΔH values between 2.1 and 20.9 kJ·mol^{-1} suggest that physical adsorption is dominant, with hydrogen bonding forces being the primary interactions between the adsorbent and adsorbate [84].

Positive ΔG values denote that the process is nonspontaneous [37]. The entropy change (ΔS) serves as an indicator of the attraction or repulsion forces within the system, relating to the spatial configuration at the adsorbent interface [41]. Positive ΔS values suggest a favorable affinity between the adsorbent and F^- ions, indicating that the randomness at the solid/solution interface increases during the F^- adsorption process [85].

CONCLUSIONS

This research examined the adsorption of fluoride (F^-) on biochar derived from coffee grounds and modified with H_2O_2 (30 vol) (FBC). The surface physicochemical characterization showed that FBC had a lower pH than pristine biochar (BCP), indicating a higher presence of acid functional groups on the FBC surface, as confirmed by FTIR analysis. The pH played a crucial role in F^- adsorption, with FBC achieving its highest adsorption capacity and removal efficiency at pH 4 (0.179 mg·g^{-1} and 25.5%, respectively), whereas BCP exhibited the highest values at pH 2.0 (0.1235 mg·g^{-1} and 20.6%, respectively). The kinetic analysis revealed that the initial F^- concentration significantly affected the time to reach adsorption equilibrium and the maximum adsorption capacity. The pseudo-second-order and Elovich models provided the best fit for the kinetic data of both adsorbents, indicating that chemical mechanisms predominated in the adsorption process. Furthermore, the intraparticle diffusion model indicated that FBC's F^- adsorption occurred in three stages, with intraparticle diffusion being the rate-limiting step. As both chemical and physical interaction were involved, the adsorption isotherms were well-represented by both Langmuir and Freundlich models. The maximum adsorption capacities for F^- in BCP and FBC were 1.46 mg·g^{-1} and 0.26 mg·g^{-1}, respectively, at 55 °C. The adsorption process was determined to be endothermic and nonspontaneous for both adsorbents, affecting their affinity for F^-.

Acknowledgments

The authors gratefully acknowledge the financial support provided by the National Health Foundation (FUNASA) through the TED 02/2018 for the development of the research.

REFERENCES

1. Rahmati O, Naghibi SA, Shahabi H, et al. 2018. Groundwater spring potential modelling: Comprising the capability and robustness of three different modeling approaches. J Hydrol 565:248–261. https://doi.org/10.1016/j.jhydrol.2018.08.027
2. Ali S, Fakhri Y, Golbini M, et al. 2019. Concentration of fluoride in groundwater of India: A systematic review, meta-analysis and risk assessment. Groundwater Sustainable Dev 9:100224. https://doi.org/10.1016/j.gsd.2019.100224
3. Khosravi K, Barzegar R, Miraki S, et al. 2020. Stochastic modeling of groundwater fluoride contamination: Introducing lazy learners. Groundwater 58: 723–734. https://doi.org/10.1111/gwat.12963
4. WHO. 2021 Guidelines for drinking-water quality, 4th edition, incorporating the 1st addendum. https://www.who.int/publications-detail-redirect/9789241549950. Accessed 24 Apr 2024
5. Liu L, Wu J, He S, Wang L. 2022. Occurrence and distribution of groundwater fluoride and manganese in the Weining Plain (China) and their probabilistic health risk quantification. Expo Health 14: 263–279. https://doi.org/10.1007/s12403-021-00434-4
6. McMahon PB, Brown CJ, Johnson TD, et al. 2020. Fluoride occurrence in United States groundwater. Sci Total Environ 732: 139217. https://doi.org/10.1016/j.scitotenv.2020.139217
7. Martins VT de S, Pino DS, Bertolo R, et al. 2018. Who to blame for groundwater fluoride anomaly in São Paulo, Brazil? Hydrogeochemistry and isotopic evidence. Appl Geochem 90:25–38. https://doi.org/10.1016/j.apgeochem.2017.12.020
8. Luo Q, Lei Y, Chen J, et al. 2020. Treatment of High Fluorine Surface Water by Crystal Seed Method. IOP Conf Ser: Earth Environ Sci 598:012050. https://doi.org/10.1088/1755-1315/598/1/012050
9. Goncharuk VV, Deremeshko LA, Balakina MN, Kucheruk DD. 2013. Purification of waters containing fluorine by low pressure reverse osmosis for their

complex treatment. J Water Chem Technol 35:122–127. https://doi.org/10.3103/S1063455X13030053

10. Wang H, Zhong H, Liu L, Quan B. 2017. Defluoridation effect for high fluorine geothermal water using electric flocculation method. Nat Environ Pollut tech 16.
11. Djouadi Belkada F, Kitous O, Drouiche N, et al. 2018. Electrodialysis for fluoride and nitrate removal from synthesized photovoltaic industry wastewater. Sep Purif Technol 204: 108–115. https://doi.org/10.1016/j.seppur.2018.04.068
12. Ni C, Liu C, Xie Y, et al. 2022. A critical review on adsorption and recovery of fluoride from wastewater by metal-based adsorbents. Environ Sci Pollut Res 29: 82740–82761. https://doi.org/10.1007/s11356-022-23416-8
13. Ravancic ME, Habuda-Stanic M. 2015. Equilibrium and kinetics studies for the adsorption of fluoride onto commercial activated carbons using fluoride ion- selective electrode. Int J Electrochem Sci 10: 8137–8149. https://doi.org/10.1016/S1452-3981(23)11082-0
14. Bhatnagar A, Kumar E, Sillanpää M. 2011. Fluoride removal from water by adsorption—A review. Chemical Engineering Journal 171: 811–840. https://doi.org/10.1016/j.cej.2011.05.028
15. Thompson KA, Shimabuku KK, Kearns JP, et al. 2016. Environmental comparison of biochar and activated carbon for tertiary wastewater treatment. Environ Sci Technol 50: 11253–11262. https://doi.org/10.1021/acs.est.6b03239
16. Cheng N, Wang B, Wu P, et al. 2021. Adsorption of emerging contaminants from water and wastewater by modified biochar: A review. Environmental Pollution 273: 116448. https://doi.org/10.1016/j.envpol.2021.116448
17. Dai Y, Zhang N, Xing C, et al. 2019. The adsorption, regeneration and engineering applications of biochar for removal organic pollutants: A review. Chemosphere 223: 12–27. https://doi.org/10.1016/j.chemosphere.2019.01.161
18. Moreira MT, Noya I, Feijoo G. 2017. The prospective use of biochar as adsorption matrix – A review from a lifecycle perspective. Bioresource Technology 246: 135–141. https://doi.org/10.1016/j.biortech.2017.08.041
19. Dong Q, Yang D, Luo L, et al. 2021. Engineering porous biochar for capacitive fluorine removal. Separation and Purification Technology 257: 117932. https://doi.org/10.1016/j.seppur.2020.117932
20. Luo Z, Yao B, Yang X, et al. 2022. Novel insights into the adsorption of organic contaminants by biochar: A review. Chemosphere 287:132113. https://doi.org/10.1016/j.chemosphere.2021.132113
21. Murtaza G, Ahmed Z, Dai D-Q, et al. 2022. A review of mechanism and adsorption capacities of biochar-based engineered composites for removing aquatic pollutants from contaminated water. Front Environ Sci 10. https://doi.org/10.3389/fenvs.2022.1035865
22. Castiglioni M, Rivoira L, Ingrando I, et al. 2021. Characterization techniques as supporting tools for the interpretation of biochar adsorption efficiency in water treatment: A critical review. Molecules 26:5063. https://doi.org/10.3390/molecules26165063
23. Cherdchoo W, Nithettham S, Charoenpanich J. 2019. Removal of Cr(VI) from synthetic wastewater by adsorption onto coffee ground and mixed waste tea. Chemosphere 221: 758–767. https://doi.org/10.1016/j.chemosphere.2019.01.100
24. Shin J, Kwak J, Kim S, et al. 2023. Enhanced selectivity and recovery of phosphate and nitrate ions onto coffee ground waste biochars via co-precipitation of Mg/Al layered double hydroxides: A potential slow-release fertilizer. Environ Res 231: 116266. https://doi.org/10.1016/j.envres.2023.116266
25. Shin H, Tiwari D, Kim D-J. 2020. Phosphate adsorption/desorption kinetics and P bioavailability of Mg-biochar from ground coffee waste. J Water Process Eng 37: 101484. https://doi.org/10.1016/j.jwpe.2020.101484
26. Lee K-T, Du J-T, Chen W-H, et al. 2021. Green additive to upgrade biochar from spent coffee grounds by torrefaction for pollution mitigation. Environ Pollut 285: 117244. https://doi.org/10.1016/j.envpol.2021.117244
27. Kwak J, Lee S-H, Shin J, et al. 2022. Synthesis and applications of bismuth-impregnated biochars originated from spent coffee grounds for efficient adsorption of radioactive iodine: A mechanism study. Environ Pollut 313: 120138. https://doi.org/10.1016/j.envpol.2022.120138
28. dos Santos HVR, Scalize PS, Teran FJC, Cuba RMF. 2023. Fluoride removal from aqueous medium using biochar produced from coffee ground. Resources 12: 84. https://doi.org/10.3390/resources12070084
29. Ogata F, Tominaga H, Yabutani H, Kawasaki N. 2011. Removal of fluoride ions from water by adsorption onto carbonaceous materials produced from coffee grounds. J Oleo Sci 60: 619–625. https://doi.org/10.5650/jos.60.619
30. Usevičiūtė L, Baltrėnaitė-Gedienė E, Baltrėnas P. 2021. Hydrophilicity enhancement of low-temperature lignocellulosic biochar modified by physical–chemical techniques. J Mater Cycles Waste Manag 23: 1838–1854. https://doi.org/10.1007/s10163-021-01255-y
31. Zhang Y, Zheng Y, Yang Y, et al. 2021. Mechanisms and adsorption capacities of hydrogen peroxide modified ball milled biochar for the removal of methylene blue from aqueous solutions. Bioresource

Technology 337. https://doi.org/10.1016/j.biortech.2021.125432

32. Tomczyk A, Szewczuk-Karpisz K. 2022. Effect of biochar modification by vitamin C, hydrogen peroxide or silver nanoparticles on its physicochemistry and tetracycline removal. Materials (Basel) 15:5379. https://doi.org/10.3390/ma15155379
33. Tan Z, Zhang X, Wang L, et al. 2019. Sorption of tetracycline on H_2O_2-modified biochar derived from rape stalk. Environ Pollut Bioavailability 31: 198–207. https://doi.org/10.1080/26395940.2019.1607779
34. Standard Methods. In: Standard Methods for the Examination of Water and Wastewater. https://www.standardmethods.org/. Accessed 25 Oct 2023
35. Alves ACF, Antero RVP, de Oliveira SB, et al. 2019. Activated carbon produced from waste coffee grounds for an effective removal of bisphenol-A in aqueous medium. Environ Sci Pollut Res 26: 24850–24862. https://doi.org/10.1007/s11356-019-05717-7
36. Huff MD, Lee J.W. 2016. Biochar-surface oxygenation with hydrogen peroxide. Journal of Environmental Management 165: 17–21. https://doi.org/10.1016/j.jenvman.2015.08.046
37. Liu W-J, Zeng F-X, Jiang H, Zhang X-S. 2011. Preparation of high adsorption capacity bio-chars from waste biomass. Bioresour Technol 102: 8247–8252. https://doi.org/10.1016/j.biortech.2011.06.014
38. Choi M-Y, Lee C-G, Park S-J. 2022. Enhanced fluoride adsorption on aluminum-impregnated kenaf biochar: adsorption characteristics and mechanism. Water Air Soil Pollut 233: 435. https://doi.org/10.1007/s11270-022-05906-0
39. Daifullah A.A.M, Yakout SM, Elreefy SA. 2007. Adsorption of fluoride in aqueous solutions using KMnO4-modified activated carbon derived from steam pyrolysis of rice straw. J Hazard Mater 147: 633–643. https://doi.org/10.1016/j.jhazmat.2007.01.062
40. Zhang X, Qi Y, Chen Z, et al. 2021. Evaluation of fluoride and cadmium adsorption modification of corn stalk by aluminum trichloride. Appl Surf Sci 543: 148727. https://doi.org/10.1016/j.apsusc.2020.148727
41. Huang H, Zheng Y, Wei D, et al. 2022. Efficient removal of pefloxacin from aqueous solution by acid-alkali modified sludge-based biochar: adsorption kinetics, isotherm, thermodynamics, and mechanism. Environ Sci Pollut Res Int 29: 43201–43211. https://doi.org/10.1007/s11356-021-18220-9
42. Cibati A, Foereid B, Bissessur A, Hapca S. 2017. Assessment of *Miscanthus* × *giganteus* derived biochar as copper and zinc adsorbent: Study of the effect of pyrolysis temperature, pH and hydrogen peroxide modification. J Cleaner Prod 162: 1285–1296. https://doi.org/10.1016/j.jclepro.2017.06.114
43. Sajjadi B, Zubatiuk T, Leszczynska D, et al. 2019. Chemical activation of biochar for energy and environmental applications: a comprehensive review. Rev Chem Eng 35: 777–815. https://doi.org/10.1515/revce-2018-0003
44. Roy S, Sengupta S, Manna S, Das P. 2018. Chemically reduced tea waste biochar and its application in treatment of fluoride containing wastewater: Batch and optimization using response surface methodology. Process Safety and Environmental Protection 116: 553–563. https://doi.org/10.1016/j.psep.2018.03.009
45. Sadhu M, Bhattacharya P, Vithanage M, Padmaja Sudhakar P. 2021. Adsorptive removal of fluoride using biochar – A potential application in drinking water treatment. Sep Purif Technol 278: 119106. https://doi.org/10.1016/j.seppur.2021.119106
46. Ke Y, Cui S, Fu Q, et al. 2022. Effects of pyrolysis temperature and aging treatment on the adsorption of Cd^{2+} and Zn^{2+} by coffee grounds biochar. Chemosphere 296: 134051. https://doi.org/10.1016/j.chemosphere.2022.134051
47. Pandey D, Daverey A, Dutta K, et al. 2022. Valorization of waste pine needle biomass into biosorbents for the removal of methylene blue dye from water: Kinetics, equilibrium and thermodynamics study. Environ Technol Innovation 25: 102200. https://doi.org/10.1016/j.eti.2021.102200
48. Cui S, Shan Y, Liu Y. 2021. Hg0 Removal by Straw Biochars Prepared with Clean Microwave/H_2O_2 Modification. Chemical Engineering & Technology 44:1460–1469. https://doi.org/10.1002/ceat.202100009
49. Shin J, Lee S-H, Kim S, et al. 2021. Effects of physicochemical properties of biochar derived from spent coffee grounds and commercial activated carbon on adsorption behavior and mechanisms of strontium ions (Sr^{2+}). Environ Sci Pollut Res 28:40623–40632. https://doi.org/10.1007/s11356-020-10095-6
50. Wei Y, Wang L, Li H, et al. 2022. Synergistic fluoride adsorption by composite adsorbents synthesized from different types of materials – A review. Front Chem 10. https://doi.org/10.3389/fchem.2022.900660
51. Thommes M, Kaneko K, Neimark AV, et al. 2015. Physisorption of gases, with special reference to the evaluation of surface area and pore size distribution (IUPAC Technical Report). Pure Appl Chem 87: 1051–1069. https://doi.org/10.1515/pac-2014-1117
52. Xue Y, Gao B, Yao Y, et al. 2012. Hydrogen peroxide modification enhances the ability of biochar (hydrochar) produced from hydrothermal carbonization of peanut hull to remove aqueous heavy metals: Batch and column tests. Chemical Engineering Journal 200–202: 673–680. https://doi.org/10.1016/j.cej.2012.06.116

53. Yakout SM, Salem NA, Mostafa AA, Abdeltawab AA. 2019. Relation between biochar physicochemical characteristics on the adsorption of fluoride, nitrite, and nitrate anions from aqueous solution. Part Sci Technol 37: 118–122. https://doi.org/10.1080/02726351.2017.1352633
54. Araga R, Kali S, Sharma CS. 2019. Coconut-shell-derived carbon/carbon nanotube composite for fluoride adsorption from aqueous solution. CLEAN – Soil, Air, Water 47: 1800286. https://doi.org/10.1002/clen.201800286
55. Sha Q, Xie H, Liu W, et al. 2023. Removal of fluoride using platanus acerifoli leaves biochar - an efficient and low-cost application in wastewater treatment. Environ Technol 44: 93–107. https://doi.org/10.1080/09593330.2021.1964002
56. Oh T-K, Choi B, Shinogi Y, Chikushi J. 2012. Effect of pH conditions on actual and apparent fluoride adsorption by biochar in aqueous phase. Water Air Soil Pollut 223: 3729–3738. https://doi.org/10.1007/s11270-012-1144-2
57. Jeyaseelan A, Mezni A, Viswanathan N. 2022. Facile hydrothermal fabrication of functionalized multilayer graphene oxide encapsulated chitosan beads for enriched fluoride adsorption. J Appl Polym Sci 139: 51703. https://doi.org/10.1002/app.51703
58. Bhaumik R, Mondal NK. 2015. Adsorption of fluoride from aqueous solution by a new low-cost adsorbent: thermally and chemically activated coconut fibre dust. Clean Techn Environ Policy 17: 2157–2172. https://doi.org/10.1007/s10098-015-0937-6
59. Biliani SE, Vakros J, Manariotis ID. 2022. Screening of raw and modified biochars from food processing wastes for the removal of phosphates, nitrates, and ammonia from water. Sustainability 14:16483. https://doi.org/10.3390/su142416483
60. Zhou J, Liu Y, Han Y, et al. 2019. Bone-derived biochar and magnetic biochar for effective removal of fluoride in groundwater: Effects of synthesis method and coexisting chromium. Water Environ Res 91: 588–597. https://doi.org/10.1002/wer.1068
61. Kumar R, Sharma P, Yang W, et al. 2022. State-of-the-art of research progress on adsorptive removal of fluoride-contaminated water using biochar-based materials: Practical feasibility through reusability and column transport studies. Environ Res 214: 114043. https://doi.org/10.1016/j.envres.2022.114043
62. Raichur AM, Jyoti Basu M. 2001. Adsorption of fluoride onto mixed rare earth oxides. SeSep Purif Technol.paration and Purification Technology 24: 121–127. https://doi.org/10.1016/S1383-5866(00)00219-7
63. Nascimento RF do, Lima ACA de, Vidal CB, et al. 2014. Adsorção: aspectos teóricos e aplicações ambientais
64. Kumar P, Prajapati AK, Dixit S, Yadav VL. 2020. Adsorption of fluoride from aqueous solution using biochar prepared from waste peanut hull. Mater Res Express 6: 125553. https://doi.org/10.1088/2053-1591/ab6ca0
65. Fan S, Wang Y, Wang Z, et al. 2017. Removal of methylene blue from aqueous solution by sewage sludge-derived biochar: Adsorption kinetics, equilibrium, thermodynamics and mechanism. Journal of Environmental Chemical Engineering 5: 601–611. https://doi.org/10.1016/j.jece.2016.12.019
66. Chiavola A, D'Amato E, Di Marcantonio C. 2022. Comparison of adsorptive removal of fluoride from water by different adsorbents under laboratory and real conditions. Water 14: 1423. https://doi.org/10.3390/w14091423
67. Ghanbarian M, Ghanbarian M, Mahvi AH, Tabatabaie T. 2020. Enhanced fluoride removal over MgFe2O4–chitosan–CaAl nanohybrid: Response surface optimization, kinetic and isotherm study. Int J Biol Macromol 148: 574–590. https://doi.org/10.1016/j.ijbiomac.2020.01.143
68. Choong CE, Wong KT, Jang SB, et al. 2020. Fluoride removal by palm shell waste based powdered activated carbon vs. functionalized carbon with magnesium silicate: Implications for their application in water treatment. Chemosphere 239: 124765. https://doi.org/10.1016/j.chemosphere.2019.124765
69. Ton-That L, Huynh T-N-L, Duong B-N, et al. 2023. Kinetic studies of the removal of methylene blue from aqueous solution by biochar derived from jackfruit peel. Environ Monit Assess 195: 1266. https://doi.org/10.1007/s10661-023-11867-6
70. Biswas S, Meikap BC, Sen TK. 2019. Adsorptive removal of aqueous phase copper (Cu^{2+}) and nickel (Ni^{2+}) metal ions by synthesized biochar–biopolymeric hybrid adsorbents and process optimization by response surface methodology (RSM). Water Air Soil Pollut 230: 197. https://doi.org/10.1007/s11270-019-4258-y
71. Ghorbani-Khosrowshahi S, Behnajady MA. 2016. Chromium(VI) adsorption from aqueous solution by prepared biochar from Onopordom Heteracanthom. Int J Environ Sci Technol 13: 1803–1814. https://doi.org/10.1007/s13762-016-0978-3
72. Liu J, Yang X, Liu H, et al. 2020. Modification of calcium-rich biochar by loading Si/Mn binary oxide after NaOH activation and its adsorption mechanisms for removal of Cu(II) from aqueous solution. Colloids Surf, A 601: 124960. https://doi.org/10.1016/j.colsurfa.2020.124960
73. Yadav K, Jagadevan S. 2021. Influence of torrefaction and pyrolysis on engineered biochar and its applicability in defluoridation: Insight into adsorption mechanism, batch adsorber design and artificial neural network modelling. J Anal Appl Pyrolysis 154: 105015. https://doi.org/10.1016/j.jaap.2021.105015

74. Neeli ST, Ramsurn H, Ng CY, et al. 2020. Removal of Cr(VI), As(V), Cu(II), and Pb(II) using cellulose biochar supported iron nanoparticles: A kinetic and mechanistic study. J Environ Chem Eng 8: 103886. https://doi.org/10.1016/j.jece.2020.103886
75. Cho E-J, Kang J-K, Moon J-K, et al. 2021. Removal of triclosan from aqueous solution via adsorption by kenaf-derived biochar: Its adsorption mechanism study via spectroscopic and experimental approaches. J Environ Chem Eng 9: 106343. https://doi.org/10.1016/j.jece.2021.106343
76. Liu R-L, Liu Y, Zhou X-Y, et al. 2014. Biomass-derived highly porous functional carbon fabricated by using a free-standing template for efficient removal of methylene blue. Bioresour Technol 154: 138–147. https://doi.org/10.1016/j.biortech.2013.12.034
77. Wang H, Fang C, Wang Q, et al. 2018. Sorption of tetracycline on biochar derived from rice straw and swine manure. RSC Adv 8: 16260–16268. https://doi.org/10.1039/C8RA01454J
78. Khan BA, Ahmad M, Iqbal S, et al. 2022. Effectiveness of the engineered pinecone-derived biochar for the removal of fluoride from water. Environ Res 212: 113540. https://doi.org/10.1016/j.envres.2022.113540
79. Habibi N, Rouhi P, Ramavandi B. 2019. Modification of Tamarix hispida Biochar by Lanthanum Chloride for Enhanced Fluoride Adsorption from Synthetic and Real Wastewater. Environ Prog Sustainable Energy 38: S298–S305. https://doi.org/10.1002/ep.13026
80. Bombuwala Dewage N, Liyanage AS, Pittman CU, et al. 2018. Fast nitrate and fluoride adsorption and magnetic separation from water on α-Fe_2O_3 and Fe_3O_4 dispersed on Douglas fir biochar. Bioresour Technol 263: 258–265. https://doi.org/10.1016/j.biortech.2018.05.001
81. Yadav AK, Abbassi R, Gupta A, Dadashzadeh M. 2013. Removal of fluoride from aqueous solution and groundwater by wheat straw, sawdust and activated bagasse carbon of sugarcane. Ecol Eng 52: 211–218. https://doi.org/10.1016/j.ecoleng.2012.12.069
82. Guan X, Zhou J, Ma N, et al. 2015. Studies on modified conditions of biochar and the mechanism for fluoride removal. Desalin Water Treat 55: 440–447. https://doi.org/10.1080/19443994.2014.916230
83. Liu Z, Zhang J, Mou R. 2023. Phosphogypsum-Modified Vinasse Shell Biochar as a Novel Low-Cost Material for High-Efficiency Fluoride Removal. Molecules 28: 7617. https://doi.org/10.3390/molecules28227617
84. Ma H, Xu Z, Wang W, et al. 2019. Adsorption and regeneration of leaf-based biochar for p-nitrophenol adsorption from aqueous solution. RSC Adv 9: 39282–39293. https://doi.org/10.1039/C9RA07943B
85. Wang J, Chen N, Li M, Feng C. 2018. Efficient removal of fluoride using polypyrrole-modified biochar derived from slow pyrolysis of pomelo peel: Sorption capacity and mechanism. J Polym Environ 26: 1559–1572. https://doi.org/10.1007/s10924-017-1061-y